IJCRT.ORG ISSN : 2320-2882

INTERNATIONAL JOURNAL OF CREATIVE RESEARCH THOUGHTS (IJCRT)

An International Open Access, Peer-reviewed, Refereed Journal

Physical Characterization of Hydro-Edaphic-Metamorphic (HEM) of Bharveli Mine Area of Balaghat, (MP), India

Mayuri Tembhre[1, 2], Sunita Dayal[2], Tarachand Badghaia[3], Anil Kumar[4]

[1]Department of Chemistry, Raja Shankar Shah University, Chhindwara, MP, India.
[2]Department of Chemistry, PMCoE, Govt. P.G. College, Chhindwara, MP, India.
[3]Department of Chemistry, PMCoE, Govt. J.S.T. P.G. College, Balaghat, MP, India.
[4]Department of Botany, PMCoE, Govt. Tilak P.G. College, Katni, MP, India.

Abstract

This study examines the physical properties of HEM samples taken from metamorphic rocks (R1, R2, R3) of the Bharveli mine area, as well as soil (S) and water (W) samples from Gangulpara Lake, at three temperature conditions: 25°C, 30°C, and 35°C. Textural analysis revealed that sample R1 contained the highest amount of sand at 92.5%, while the Gangulpara soil sample contained the lowest amount of clay at 5%. pH values varied from 6.08 in R2 to 6.95 in water sample W. Electrical conductivity (EC) was highest in R2 at 586 µS/cm and lowest in W at 245 µS/cm. Density measurements ranged from a maximum of 0.9966 g/cm³ in R2 to a minimum of 0.9929 g/cm³ in W. Viscosity was highest in W at 0.8147 mPa·s and lowest in R2 at 0.6143 mPa·s. Surface tension measurements showed a similar trend, with the highest value at 85.17 mN/m in R2 and the lowest at 72.79 mN/m in W. These results provide important information about the physical properties of the material under different thermal conditions, both in mining and in lake sites.

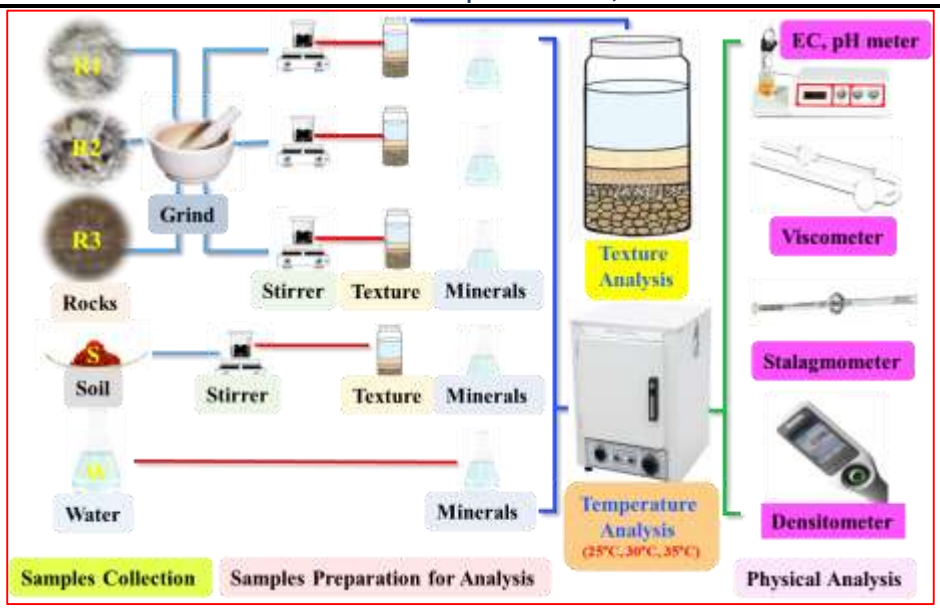

Figure 1: Graphical abstract of the schematic of research objects.

Keywords: Bharveli mine, Gangulpara Lake, Temperature, Texture, pH, Electrical conductivity, Density, Viscosity, Surface tension.

Introduction

Mountains, composed primarily of igneous and metamorphic rocks, are a natural source of minerals essential for the recharge of agricultural land [1, 2]. Through processes such as weathering, erosion, rain leaching, snowmelt, and glacial runoff, these rocks release macronutrients such as calcium, magnesium, potassium, and phosphorus and micronutrients including iron, zinc, manganese, copper, and boron to surrounding ecosystems [3, 4]. Glaciers and icebergs in mountainous regions act as seasonal reservoirs, slowly releasing mineral-rich meltwater that feeds rivers, lakes, and groundwater systems [5, 6]. This water contains important chemical compounds such as carbonates for pH regulation, silicates, a source of silica, sulfates, and nitrates for plant nutrition, and trace metals essential for enzymatic and plant processes [7]. As this water flows downhill, it deposits nutrient-rich silt and sediment, providing naturally fertile irrigation to agricultural lands, as seen in the Ganges River from the Himalayas and the Nile River from the Ethiopian highlands [8, 9]. Scientific studies emphasize the global importance of mountains in maintaining soil fertility and agriculture [10, 11]. According to the FAO, mountain regions supply 60-80% of the worlds freshwater, which also contains nutrients essential for lowland agriculture [12-14]. NASA has confirmed that melting mountains improves the quality of lower-lying soils by delivering dissolved minerals [15]. The USGS states that sediment carried by Mountain Rivers contributes up to 50% to soil fertility in valleys, while the Journal of Hydrology reports that mountain-based irrigation systems can increase crop yields by 20-40% due to the increased availability of micronutrients [16-18]. In India, Himalayan rivers deliver 30-50 million tonnes of mineral-rich sediments annually to the Indo-Gangetic plains [19, 20].

Mining activities at Bharveli, a strategic site of the Balaghat Mining Complex and Asia's largest underground manganese mine, have significantly altered the local hydro-climatic environment. Operating since 1903 and owned by MOIL Limited, the mine is located in a geologically rich region composed of metamorphic sedimentary rocks such as sericite schist, phyllite, feldspathic quartzite, and gritty conglomerates containing

striated manganese ore bodies [21]. Continued extraction of manganese has disrupted the physical and chemical properties of the region's soil and water, reducing water-holding capacity, altering infiltration rates, and diminishing soil fertility [22, 23]. These changes highlight the environmental impact of continued mining operations on local ecosystems. These changes result in the development of new mineral assemblages and structures, while often preserving remnants of their sedimentary origin [24, 25].

Commonly encountered metamorphic sedimentary lithologies include sericite schist, phyllite, feldspathic quartzite, and gritty conglomerates. Sericite schists are typically fine-grained, clay-rich sedimentary rocks, such as mudstones [26]. They are characterized by a foliated texture dominated by granular sericite mica, which gives them a silky luster and cleavage. Their appearance often indicates metamorphism and deformation [27]. Phyllite is a metamorphic rock that is a transitional rock between slate and schist [28]. Derived from mudstone, it has a fine-grained, foliated texture [29]. Feldspathic quartzite forms from arkosic sandstones rich in feldspar and quartz [30]. During metamorphism, these rocks crystallize into a hard, dense rock containing quartz and feldspar grains [31]. Preservation of sedimentary cross-bedding is visible, providing clues about the rock's protolith and deposition. After metamorphism, sandy conglomerates retain the rough, clastic texture of their sedimentary predecessors but exhibit crystallization and foliation around the clasts.

Hydro-Edaphic-Metamorphic (HEM) characterization involves assessing the physical properties of soil to understand their water-holding capacity, infiltration, and fertility potential [32-34]. Physical parameters include bulk and particle density, porosity, and water-holding capacity, while chemical properties evaluated include pH, electrical conductivity, and other macronutrients such as nitrogen, phosphorus, potassium, and sulfur [35-37]. A study of mining-affected soils in Balaghat revealed that these soils exhibit neutral to slightly alkaline pH, low salinity, and basic physical properties such as density, porosity, and surface tension. These results provide a comparative basis for assessing similar environmental conditions in the Bharveli mining area location indicated as R1, R2, R3, and the nearby Gangulpara Lake two samples indicated as S for soil and W for water (Figure 1).

The objective of this study is to analyze the physical and hydrological properties of mining-affected soils in Bharveli, Balaghat, focusing on indicators such as soil texture, density, porosity, water-holding capacity, pH, electrical conductivity, and macronutrient status. The assessing these parameters, the study attempts to assess the extent of soil charging profiles due to mining activities.

Materials and Methods

Study area

The Bharveli mine and Gangulpara Lake are located near the Balaghat mining area (21°50’N, 80°14’E), an area with a tropical dry savanna climate and undulating terrain within the Satpura Wainganga Valley system (Figure 2). The mine and lake are located within the Proterozoic Mansar Group geological formations, which include schists, quartzites, and conglomerates associated with manganese ore bands.

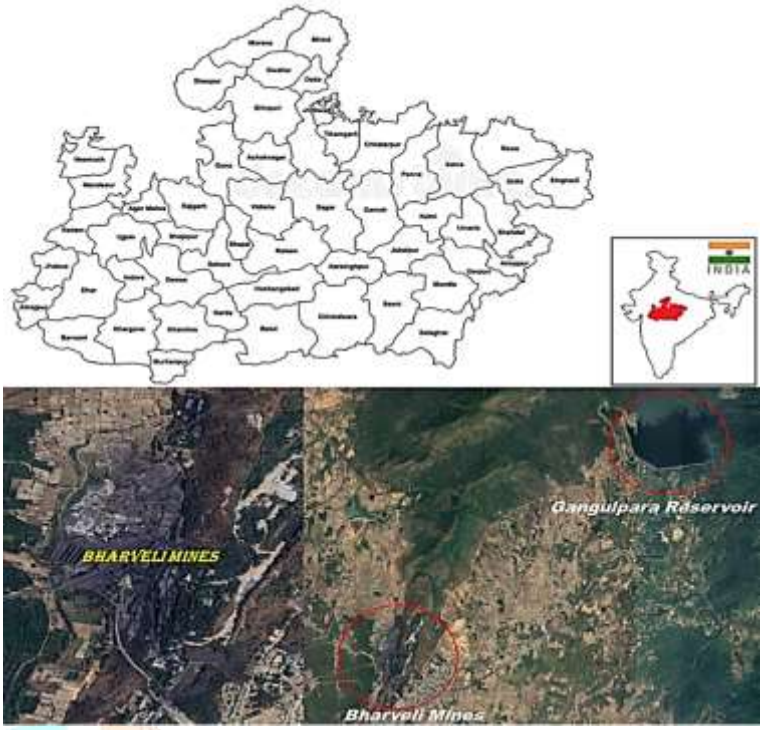

Figure 2: Maps and satellite images of the study sites.

Sample collection

Sampling sites determination locations indicated rocks (R1, R2, R3) were selected in the mining area Bharveli mine affected areas, and hydro-edaphic (water and soil) samples (S and W) were collected from the non-mining sites of Gangulpara Lake.

Metamorphic rock samples of 100 g each were collected from selected sites R1, R2, and R3 of the Bharveli mine area. Hydro-edaphic samples containing 100 g of soil (S) and 100 ml of water (W) were collected in sterile containers from Gangulpara Lake.

Laboratory analysis

A total of five sampling sites were identified and designated R1, R2, R3, S, and W. Representative soil and rock samples were collected from each site for analysis. The solid samples were first air-dried and then finely powdered using a mechanical grinder to ensure uniform particle size. After grinding, the powdered samples were dissolved in distilled water in a controlled ratio to prepare a homogeneous suspension suitable for physical testing.

Texture estimation

The determined sedimentation analysis was used to determine the relative proportions of sand, silt, and clay in soil and water from lake and rock samples collected from designated locations [38]. A total of 100 grams of each sample was collected. The rock samples were first cleaned and air-dried to remove moisture [39-41]. The rock samples were then crushed and ground into a fine powder. For dispersion, 50 grams of powdered rock and clay were placed in a beaker with 100 ml of distilled water, stirred at 250 rpm using a magnetic stirrer, and allowed to stand overnight. The dispersed mixture was transferred to cylinders, and sedimentation was monitored at specific time intervals at room temperature to calculate the particle size distribution, such as

sand (>0.05 mm), silt (0.002–0.05 mm), and clay (<0.002 mm). The soil texture is based on the relative proportions of these three components.

Physical properties estimation

The five physical parameters were measured to analyze these prepared soil and rock finely ground powder water suspension samples.

Sample preparation

After the sedimentation process was complete, a transparent upper layer of water containing dissolved minerals and fine colloidal particles was observed in each cylinder. This upper layer was carefully removed using a sterile pipette, and 50 ml of each sample was transferred to glass conical flasks labeled corresponding to the sedimentation sites (R1, R2, R3, S, and W). To avoid contamination, the collected water samples were stored in tightly closed containers and placed in a temperature-controlled chamber at 25°C for 60 minutes as part of the thermal treatment process [42]. Next, two separate sets of samples were heated in a pre-calibrated hot air oven, one set at 30°C and the other at 35°C, for an additional 60 minutes to ensure uniform heating.

pH

The pH meter was first calibrated using standard buffer solutions with pH values of 4.00, 7.00, and 10.00 [43, 44]. The electrode was immersed in each solution sequentially, rinsed with distilled water between calibrations, and the meter was adjusted accordingly. The collected mineral water samples were then transferred to clean, labeled beakers for pH measurements at three specific temperatures: 25°C, 30°C, and 35°C. The samples were brought to the desired temperature using a water bath, with a digital thermometer used to ensure precise temperature control. Before each measurement, the electrode was rinsed and gently wiped to avoid contamination. Then, it was fully immersed in the sample without air bubbles, and after stabilization, the pH reading was taken.

Electrical conductivity

The conductivity meter was first tested for proper functionality and calibrated using a standard potassium chloride solution with a known conductivity value at 25°C [45]. The conductivity probe was rinsed with distilled water and carefully dried to remove any residual impurities. Each mineral water sample was then divided into three parts and placed in separate beakers for conductivity testing at 25°C, 30°C, and 35°C. A digital thermometer was used to confirm the exact temperature of each sample before measurement. The conductivity probe was completely immersed in the solution, ensuring no air bubbles were present, and the sensing element was completely submerged [46, 47]. Gentle shaking ensured an even distribution of ions, and once the reading stabilized, the electrical conductivity was recorded in microsiemens per centimeter (µS/cm) [48]. This process was repeated for each sample at all three temperatures, and the results were carefully recorded.

Density

A clean, dry 100 ml crystallizer bottle was selected and thoroughly rinsed with distilled water, then dried in a hot air oven to remove any residual moisture [49]. The empty bottle was weighed using an analytical balance with a precision of at least 0.001 g, and this mass was recorded as m_1. Next, the bottle was filled with 50 ml of mineral water sample, and the filled bottle was weighed again to obtain m_2, which is the mass of the bottle containing the liquid sample. This arrangement was designed to determine the mass of the liquid sample by calculating the difference between m_2 and m_1 [50, 51].

$$Density\ (\rho) = \frac{Mass\ (m)}{Valume\ (V)}$$

Viscosity

The Ostwald viscometer was first thoroughly cleaned with distilled water and alcohol, then thoroughly dried to avoid contamination. Calibration was performed using distilled water at 25℃ to determine the reference viscosity, and the flow time was recorded for relative comparison [52-54]. Each liquid sample was then brought to the desired test temperatures of 25℃, 30℃, and 35℃ using a controlled water bath to ensure uniformity. A measured volume of each sample was drawn into the viscometer through the inlet without generating air bubbles, drawn above the upper mark by suction, and then allowed to flow naturally downward under the influence of gravity [55]. To determine the viscosity of the sample at each temperature, the time taken for the sample to pass between the two marked points was recorded using a stopwatch.

$$Viscosity\ (\eta) = \eta 0 * \frac{\rho * t}{\rho 0 * t0}$$

Where: viscosity of sample (η), viscosity of reference (η0), density of sample (ρ), density of reference (ρ0), time of sample (t), time of reference (t0).

Surface tension

A clean and dry stalagmometer was selected and thoroughly cleaned with distilled water, then ethanol, and then air-dried to remove any potential contaminants [56]. The instrument was first calibrated by counting the number of droplets formed from a fixed volume using a reference standard, a liquid with a known surface tension [54]. Each test liquid was then brought to target temperatures of 25℃, 30℃, and 35℃ using a temperature-controlled water bath to maintain constant test conditions. The sample was drawn to the upper mark of the stalagmometer using a suction device, and the instrument was held vertically so that the liquid could form droplets under the influence of gravity [55, 57]. The number of droplets (n) formed from the known volume was carefully counted for each temperature.

$$Surface\ tension\ (\gamma) = \gamma 0 * \frac{n0 * \rho}{n * \rho 0}$$

Where: surface tension of sample (γ), surface tension of reference (γ0), density of sample (ρ), density of reference (ρ0), drop of sample (n), drop of reference (t0).

Results and Discussions

The geology of the Bharveli mines area, which includes the Gangulpara Lake area, is primarily composed of metamorphosed sedimentary rocks such as sericite schist, phyllite, feldspathic quartzite, and gritty conglomerates. These geological formations contain ore bodies and also influence the characteristics of the lake where the water and soil samples were studied. The physical properties of these samples were analyzed at different temperatures to understand their solubility and behavior in water-based conditions.

Texture analyses

Texture analysis of soil and adequate rock powder samples from the Bharveli mine area (R1, R2, R3) and Gangulpara Lake (S) sites was conducted at three temperature levels at 25°C, 30°C, and 35°C. The facts revealed variations in sand, silt, and clay content across both sites and temperatures [39, 40]. Samples from the Bharveli mine area showed a similar sandy texture, with a higher sand content at all temperatures. At 25°C, both R1 and R2 contained 92% sand, while R3 contained 91%. Silt content ranged from 7% to 8%, and clay content ranged from 0.5% to 1%. Minor changes occurred as temperatures increased to 30°C and 35°C. At 35°C, R1 showed a slight increase in clay content, from 1% to 1.5%. Clay content increased slightly with increasing temperature, from 0.5% to 1% in R2, while sand content fluctuated slightly between 92% and 92.5%. At 30°C, R3 showed a slight decrease in sand content to 90%, while silt and clay content increased similarly, returning to nearly their previous levels at 35°C. Samples from Bharveli were coarser, with higher sand and lower clay content, indicating lower water-holding capacity and lower nutrient retention, typical of the pulverized bedrock of rocks affected by mining [38]. Soil samples from Gangulpara Lake showed a more balanced texture, with significantly lower sand content and higher silt and clay content compared to the mining area. At 25°C, the composition was 80% sand, 15% silt, and 5% clay. As the temperature increased, the sand percentage gradually decreased to 78% at 30°C and 75% at 35°C, while the silt and clay content increased. At 35°C, the clay content increased from 5% to 8%, indicating a shift toward finer-textured soil. This trend indicates that the natural soil composition and water-holding capacity of Gangulpara Lake were better than the rock dust from the Bharveli mines (Figure 3).

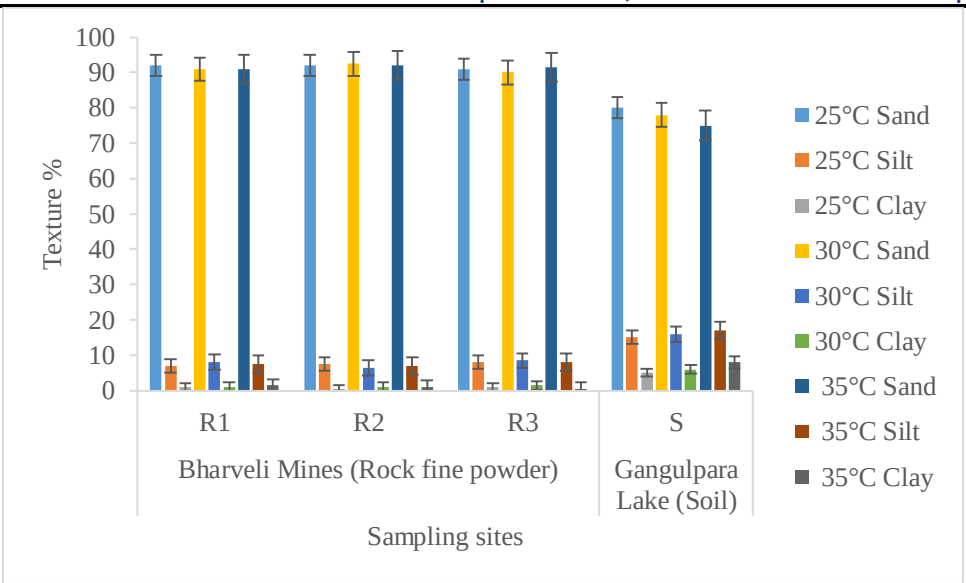

Figure 3: Texture analysis at different temperatures.

pH Analysis

Investigated the effect of temperature on the acidity or alkalinity of mineral-soluble water, the pH values of water samples taken from two different sources, the Bharveli mine and Gangulpara Lake, were measured at 25°C, 30°C, and 35°C. In all samples, the pH values decreased with increasing temperature, which is consistent with the known behavior of water due to the temperature dependence of ionization equilibrium. Three samples of rock mineral-soluble water, R1, R2, and R3, were taken from the Bharveli mine. At 25°C, the pH values were 6.62 for R1, 6.25 for R2, and 6.58 for R3. The temperature increased to 35°C, and the pH values dropped to 6.46, 6.08, and 6.32, respectively. This drop in pH reflects an increase in the spontaneous ionization of water with increasing temperature, which increases the hydrogen ion concentration and, consequently, lowers the pH value of the three samples. R2 consistently exhibited the lowest pH value at all temperatures, indicating that this sample may have a higher concentration of dissolved acidic minerals or a different chemical composition affecting its buffering capacity [44]. Soil mineral-soluble water and lake water samples were collected from Gangulpara Lake (S and W). At 25°C, the pH values were 6.66 for S and 6.95 for W. At 35°C, these values increased to 6.42 and 6.77, respectively. Compared to the samples from Bharveli, both samples from Gangulpara maintained higher pH levels, indicating a lower concentration of acidic minerals or a greater buffering effect due to soil-derived substances [43]. Sample W showed the highest pH value at all temperature points, remaining close to neutral, which may indicate relatively low mineral dissolution or a slightly alkaline character due to the natural composition of the lake (Figure 4).

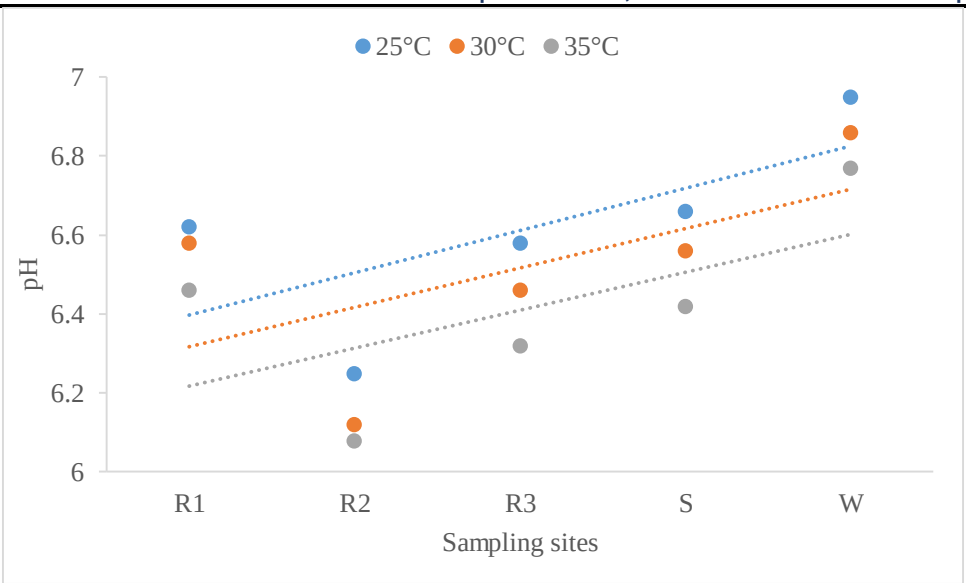

Figure 4: Effect of temperatures on pH of samples.

Electrical conductivity analysis

The electrical conductivity (EC) of water samples was measured at three different temperatures, such as 25°C, 30°C, and 35°C, to assess how ionic concentration and mobility change with temperature. EC is an important indicator of the presence of dissolved salts, minerals, and ions in water and typically increases with temperature due to increased ion mobility. Samples R1, R2, and R3 obtained from Bharveli Mines showed a steady increase in electrical conductivity with increasing temperature. The EC of sample R1 was 446 µS/cm at 25°C, which increased to 478 µS/cm at 30°C and 552 µS/cm at 35°C. Similarly, sample R2 increased from 528 µS/cm to 586 µS/cm, and R3 increased from 432 µS/cm to 546 µS/cm, over the same temperature range. This upward trend reflects both the natural increase in ion mobility with temperature and the presence of dissolved rock minerals in the samples [46]. R2 consistently had the highest EC value, indicating a higher concentration of dissolved ionic species, likely derived from soluble rock minerals in the mining area [48]. The sharp increase in R3 conductivity between 25°C and 30°C from 432 to 534 µS/cm indicated significant temperature-sensitive dissolution or ionization of some minerals. In contrast, samples S and W of Gangulpara Lake showed less consistent patterns. Sample S increased from 375 µS/cm at 25°C to 444 µS/cm at 30°C, but decreased slightly to 426 µS/cm at 35°C. This slight decrease at higher temperatures may be due to temporary ionic saturation or precipitation effects, or sample variability. Sample W, on the other hand, increased from 245 µS/cm at 25°C to 362 µS/cm at 35°C, although it remained the lowest conductivity of all samples (Figure 5). This indicates a low dissolved ionic content, which is characteristic of natural surface water with minimal mineral or pollutant influence [45].

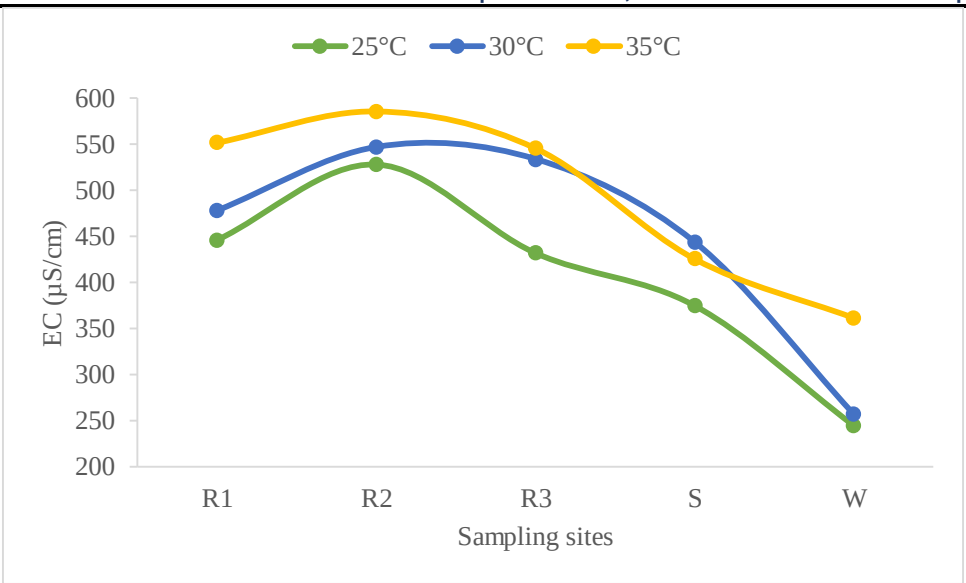

Figure 5: Effect of temperature on the electrical conductivity of different samples

Density analysis

The density of samples collected from two different locations, Bharveli Mine rock mineral soluble in water labeled (R1, R2, and R3), and Gangulpara Lake soil mineral soluble in water (S) and water (W), was analyzed at three different temperatures, such as at 25°C, 30°C, and 35°C. Bharveli Mine, three samples labeled R1, R2, and R3 were tested. The density of sample R1 was measured to be 0.9962 g/cm³ at 25°C, which decreased to 0.9947 g/cm³ at 30°C, and further decreased to 0.9934 g/cm³ at 35°C. Similarly, sample R2 showed a density of 0.9966 g/cm³ at 25°C, which decreased to 0.9949 g/cm³ at 30°C and then further decreased to 0.9937 g/cm³ at 35°C. Sample R3 also showed a similar trend, with densities of 0.9963 g/cm³, 0.9948 g/cm³, and 0.9935 g/cm³ at 25°C, 30°C, and 35°C, respectively. These results indicate that mineral-soluble water samples exhibit a consistent decrease in density with increasing temperature. In the case of Gangulpara Lake, two samples (soil mineral-soluble water S and water W) were analyzed, labeled S and W. Sample S had a density of 0.9961 g/cm³ at 25°C, which decreased to 0.9942 g/cm³ at 30°C and 0.9932 g/cm³ at 35°C. Sample W showed a slightly lower initial density of 0.9958 g/cm³ at 25°C, which decreased to 0.9936 g/cm³ at 30°C and 0.9929 g/cm³ at 35°C (Figure 6). The densities of these soil mineral-soluble water for S, and water for W, also showed a clear decrease with increasing temperature [50].

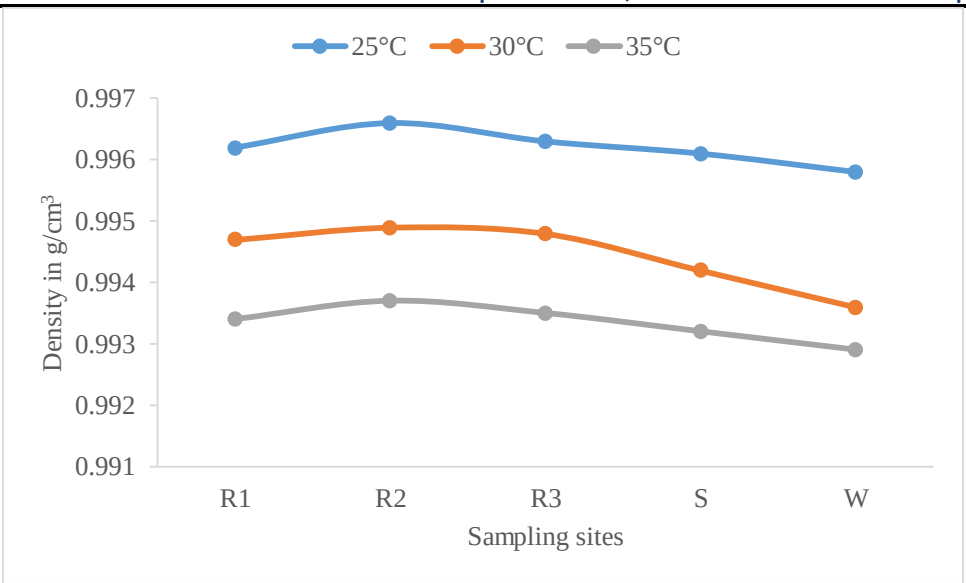

Figure 6: Density analysis with different temperatures.

Viscosity and time analysis

The effect of temperature on fluid resistance and flow behavior, the viscosity and flow time of water samples were measured at 25°C, 30°C, and 35°C. As expected, in all cases, viscosity decreased with increasing temperature, which is consistent with the normal physical behavior of liquids. Three samples of rock mineral-soluble water, R1, R2, and R3, were taken from the Bharveli mine. At 25°C, the viscosity values were 0.7126 mPa·s for R1, 0.6331 mPa·s for R2, and 0.6477 mPa·s for R3. These values steadily decreased as the temperature increased to 30°C and then to 35°C. At 35°C, R1 decreased to 0.6343 mPa·s, R2 decreased to 0.6143 mPa·s, and R3 decreased to 0.6343 mPa·s. Flow time, which indicates the time it takes for a liquid to pass through a capillary cavity, also decreased with increasing temperature. The flow time of sample R1 was 120 seconds at 25°C, which decreased to 93 seconds at 35°C. The same trend was observed for R2 and R3, indicating that water became less viscous and more mobile at higher temperatures. These observations are consistent with the physical principle that increasing temperature increases the kinetic energy of molecules, weakens intermolecular forces, and thus reduces flow resistance [54, 55]. The expected trend of decreasing viscosity with increasing temperature was observed in soil mineral-soluble water as S and lake water as W samples collected from Gangulpara Lake. At 25°C, the viscosities of Sample S and W were 0.7635 mPa·s and 0.8147 mPa·s, respectively, the highest of all samples. This suggests the presence of dissolved clay organic matter, which could have increased intermolecular friction. The temperature increased to 30°C and 35°C, the viscosity of Sample S decreased to 0.7024 mPa·s, while that of Sample W decreased to 0.7567 mPa·s. Similarly, their flow times also decreased significantly, with the Sample W flow time at 25°C decreasing from 105 seconds to only 78 seconds at 35°C (Figure 7). This confirmed the conclusion that the thermal decrease in viscosity occurred regardless of mineral content.

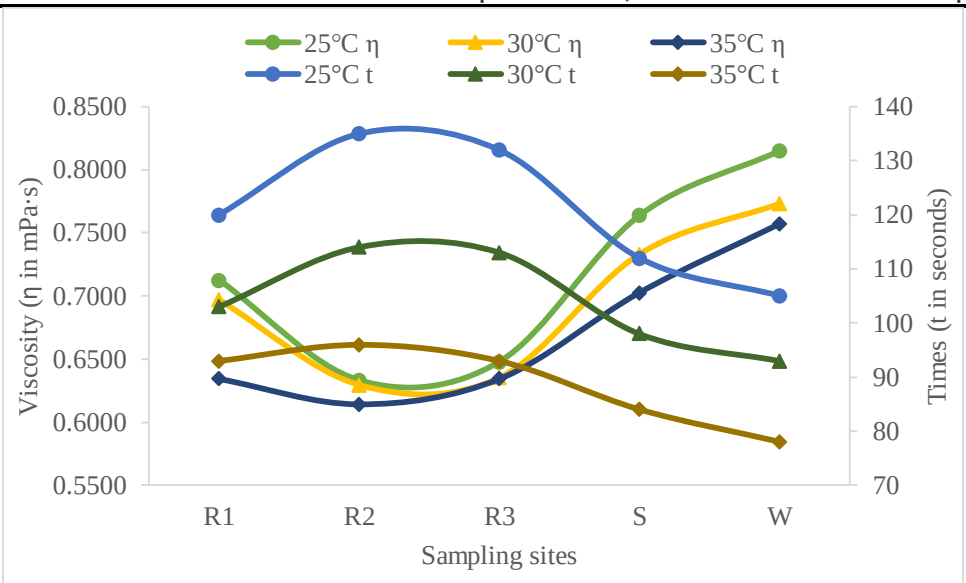

Figure 7: Analysis of viscosity vs. time at variable temperatures.

Surface tension and droplet number analysis

In this study, variations in surface tension and droplet number of water samples collected from two locations, the Bharveli Mine and Gangulpara Lake, were investigated under the same temperature conditions explained above. Rock mineral-soluble in water samples labeled R1, R2, and R3 were collected from the Bharveli Mine. In all three samples, surface tension increased with increasing temperature, contrary to the general trend observed for pure water. In sample R1, the surface tension increased from 75.89 mN/m at 25°C to 77.72 mN/m at 30°C, and then to 81.92 mN/m at 35°C. A similar increase was observed in R2, where the surface tension increased from 80.18 mN/m at 25°C to 85.17 mN/m at 35°C. In R3, the surface tension ranged from 78.42 mN/m to 82.71 mN/m at the same temperature. The number of droplets formed per unit volume also increased with temperature in all three samples. In R1, the number of droplets increased from 93 at 25°C to 104 at 35°C, indicating that smaller droplets formed at higher temperatures. This inverse relationship between droplet size and number supports the typical behavior of water under thermal influence, although the surface tension data indicated possible interference from dissolved rock minerals, which could potentially alter intermolecular forces [54]. Soil mineral-soluble water as S and lake water as W samples were collected from Gangulpara Lake. Both samples S and W showed an increase in surface tension with temperature, which differed from the expected behavior of pure water [56, 57]. The surface tension of sample S was 74.30 mN/m at 25°C, which increased to 79.64 mN/m at 35°C. Similarly, for sample W, the surface tension value increased from 72.79 mN/m to 76.11 mN/m over the same temperature range. The number of droplets increased steadily with temperature. Sample S showed an increase from 95 droplets at 25°C to 107 droplets at 35°C, while W showed a more pronounced increase from 97 to 112 droplets (Figure 8).

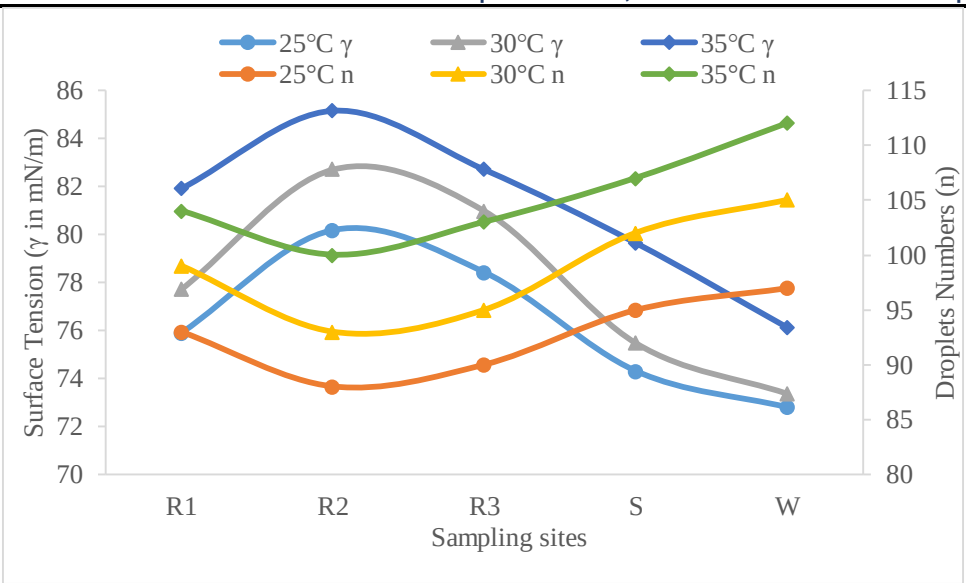

Figure 8: Surface tension and droplet analysis at variable temperatures.

Viscosity vs. Surface tension

At temperatures of 25°C, 30°C, and 35°C, the showed a similar trend of decreasing viscosity (η in mPa s) and increasing surface tension (γ in mN/m) for all samples. For R1, the viscosity decreased from 0.7126 mPa s at 25°C to 0.6343 mPa s at 35°C, while the surface tension increased from 75.8950 mN/m to 81.9222 mN/m. R2 showed a similar trend, with viscosity decreasing from 0.6331 mPa s to 0.6143 mPa s, and surface tension increasing from 80.1750 mN/m to 85.1734 mN/m. The viscosity of R3 decreased slightly from 0.6477 mPa·s to 0.6343 mPa·s, while its surface tension increased from 78.4169 mN/m to 82.7093 mN/m. Sample S showed a greater decrease in viscosity from 0.7635 mPa·s to 0.7024 mPa·s, while its surface tension increased from 74.3047 mN/m to 79.6414 mN/m. Finally, W, which initially had the highest viscosity of 0.8147 mPa·s, decreased to 0.7567 mPa·s at 35°C, and its surface tension increased from 72.7945 mN/m to 76.1090 mN/m. All samples showed expected rheological behavior, with viscosity decreasing and surface tension increasing as temperature increased (Figure 9).

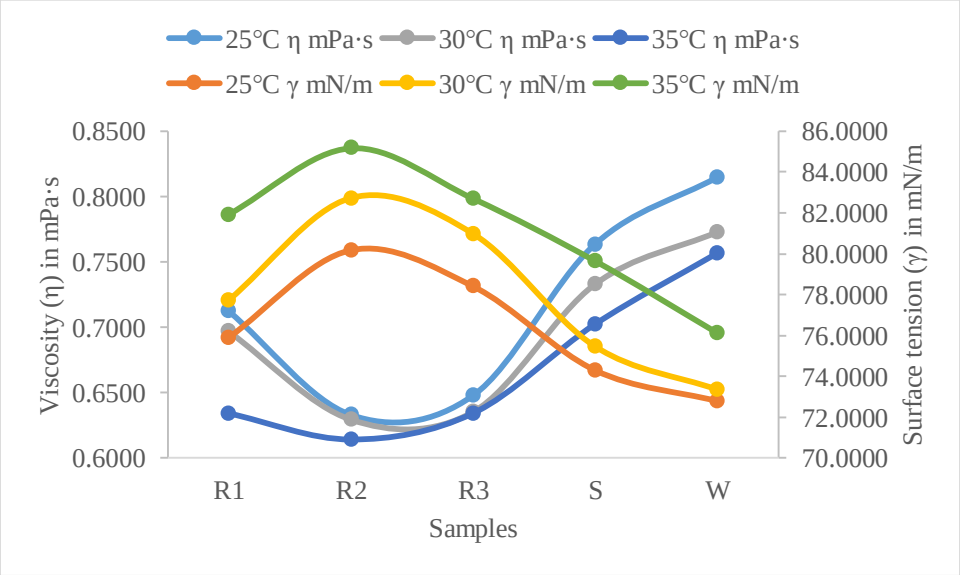

Figure 9: Viscosity vs. Surface tension analysis at variable temperatures.

Conclusion

These results show a clear difference between the mineral-rich, thermally sensitive water of the Bharveli mining zone and the more stable, naturally protected water of Gangulpara Lake. This provides insight into the impact of mining on water quality on improving soil quality by recharging the soil with minerals near the mining zone.

References

[1]. Briški, M., Stroj, A., Kosović, I., & Borović, S. (2020). Characterization of aquifers in metamorphic rocks by combined use of electrical resistivity tomography and monitoring of spring hydrodynamics. Geosciences, 10(4), 137.

[2]. Sidibé, A. M., Lin, X., & Koné, S. (2019). Assessing groundwater mineralization process, quality, and isotopic recharge origin in the Sahel region in Africa. Water, 11(4), 789.

[3]. Hahm, W. J., Riebe, C. S., Lukens, C. E., & Araki, S. (2014). Bedrock composition regulates mountain ecosystems and landscape evolution. Proceedings of the National Academy of Sciences, 111(9), 3338–3343.

[4]. Latif, Y., Ma, Y., Ma, W., Muhammad, S., Adnan, M., Yaseen, M., & Fealy, R. (2020). Differentiating snow and glacier melt contribution to runoff in the Gilgit River Basin via degree-day modelling approach. Atmosphere, 11(10), 1023.

[5]. Wadham, J. L., Hawkings, J. R., Tarasov, L., Gregoire, L. J., Spencer, R. G. M., Gutjahr, M., Ridgwell, A., & Kohfeld, K. E. (2019). Ice sheets matter for the global carbon cycle. Nature Communications, 10(1), 3567.

[6]. Zhang, Q., Chen, Y., Li, Z., Fang, G., Xiang, Y., Li, Y., & Ji, H. (2020). Recent changes in water discharge in snow and glacier melt-dominated rivers in the Tienshan Mountains, Central Asia. Remote Sensing, 12(17), 2704.

[7]. Cannas, D., Loi, E., Serra, M., Firinu, D., Valera, P., & Zavattari, P. (2020). Relevance of essential trace elements in nutrition and drinking water for human health and autoimmune disease risk. Nutrients, 12(7), 2074.

[8]. Meshesha, T., & Tripathi, S. (2015). Watershed management in highlands of Ethiopia: A review. OALib, 2, 1–11.

[9]. Gebrehiwot, K. (2018). A review on waterlogging, salinization and drainage in Ethiopian irrigated agriculture. Sustainable Water Resources Management, 4, 55–62.

[10]. Mazzocchi, C., & Sali, G. (2022). Tourists' perception of ecosystem services provided by mountain agriculture. Sustainability, 14(19), 12171.

[11]. Sobhy, D. M., & Anandhi, A. (2025). Soil nutrient monitoring technologies for sustainable agriculture: A systematic review. Sustainability, 17(18), 8477.

[12]. Du, J., Laghari, Y., Wei, Y.-C., Wu, L., He, A.-L., Liu, G.-Y., Yang, H.-H., Guo, Z.-Y., & Leghari, S. J. (2024). Groundwater depletion and degradation in the North China Plain: Challenges and mitigation options. Water, 16(2), 354.

[13]. Bănăduc, D., Simić, V., Cianfaglione, K., Barinova, S., Afanasyev, S., Öktener, A., McCall, G., Simić, S., & Curtean-Bănăduc, A. (2022). Freshwater as a sustainable resource and generator of secondary resources in the 21st century: Stressors, threats, risks, management and protection strategies, and conservation approaches. International Journal of Environmental Research and Public Health, 19(24), 16570.

[14]. Näschen, K., Diekkrüger, B., Evers, M., Höllermann, B., Steinbach, S., & Thonfeld, F. (2019). The impact of land use/land cover change (LULCC) on water resources in a tropical catchment in Tanzania under different climate change scenarios. Sustainability, 11(24), 7083.

[15]. Beyssac, O., Forni, O., Cousin, A., Udry, A., Kah, L. C., Mandon, L., et al. (2023). Petrological traverse of the olivine cumulate Séítah formation at Jezero crater, Mars: A perspective from SuperCam onboard Perseverance. Journal of Geophysical Research: Planets, 128, e2022JE007638.

[16]. Tingey, S., Wadham, J. L., Telling, J., Flynn, S., Hawkings, J. R., Palinkas, S. S., Mun, Y., Yates, C. A., Lamarche-Gagnon, G., Burford, R., Ramanathan, A. L., Hetherington, A., Dodd, A. N., Liu, X., & Sgouridis, F. (2024). The potential for glacial flour to impact soil fertility, crop yield and nutrition in mountain regions. iScience, 28(1), 111476.

[17]. Thomas, J., Joseph, S., & Thrivikramji, K. P. (2018). Assessment of soil erosion in a tropical mountain river basin of the southern Western Ghats, India using RUSLE and GIS. Geoscience Frontiers, 9(3), 893–906.

[18]. Raff, J. L., Goodbred, S. L., Pickering, J. L., et al. (2023). Sediment delivery to sustain the Ganges-Brahmaputra delta under climate change and anthropogenic impacts. Nature Communications, 14, 2429.

[19]. Garzanti, E., Andò, S., France-Lanord, C., Censi, P., Vignola, P., Galy, V., & Lupker, M. (2011). Mineralogical and chemical variability of fluvial sediments: 2. Suspended-load silt (Ganga–Brahmaputra, Bangladesh). Earth and Planetary Science Letters, 302(1–2), 107–120.

[20]. West, A. J., Bickle, M. J., Collins, R., & Brasington, J. (2002). Small-catchment perspective on Himalayan weathering fluxes. Geology, 30(4), 355–358.

[21]. Manekar, G. G., Shome, D., & Jha, A. K. (2015). Strata control for mechanized stopping operation in narrow and weak manganese deposit of MOIL – A case study of Balaghat Mine. Procedia Earth and Planetary Science, 11, 456–463.

[22]. Wu, R., Yao, F., Li, X., Shi, C., Zang, X., Shu, X., Liu, H., & Zhang, W. (2022). Manganese pollution and its remediation: A review of biological removal and promising combination strategies. Microorganisms, 10(12), 2411.

[23]. Lal, R. (2015). Restoring soil quality to mitigate soil degradation. Sustainability, 7(5), 5875–5895.

[24]. Christiansen, B., Denda, A., & Christiansen, S. (2020). Potential effects of deep seabed mining on pelagic and benthopelagic biota. Marine Policy, 114, 103442.

[25]. Tibby, J., Marshall, J. C., Short, J., Cadd, H. R., Hansen, J., Lewis, T. M., Donnellan, C. (2024). Retrospective assessment of mine impacts: A case study using palaeoecology, aerial photography and

maps from North Stradbroke Island (Minjerribah), Australia. Australasian Journal of Environmental Management, 31(3), 310–338.

[26]. Guo, H., Shi, J., Fu, S., Liu, Z., Cai, L., & Yin, S. (2024). Lithofacies characteristics of continental lacustrine fine-grained sedimentary rocks and their coupling relationship with sedimentary environments: Insights from the Shahejie Formation, Dongying Sag. Minerals, 14(5), 479.

[27]. Brown, M. (2014). The contribution of metamorphic petrology to understanding lithosphere evolution and geodynamics. Geoscience Frontiers, 5(4), 553–569.

[28]. Han, S., & Jung, H. (2021). Deformation microstructures of phyllite in Gunsan, Korea, and implications for seismic anisotropy in continental crust. Minerals, 11(3), 294.

[29]. Özbek, A., Gül, M., Karacan, E., & Alca, Ö. (2018). Anisotropy effect on strengths of metamorphic rocks. Journal of Rock Mechanics and Geotechnical Engineering, 10(1), 164–175.

[30]. Nutman, A. P., Maciejowski, R., & Wan, Y. (2014). Protoliths of enigmatic Archaean gneisses established from zircon inclusion studies: Case study of the Caozhuang quartzite, E. Hebei, China. Geoscience Frontiers, 5(4), 445–455.

[31]. Hasterok, D., Gard, M., & Webb, J. (2018). On the radiogenic heat production of metamorphic, igneous, and sedimentary rocks. Geoscience Frontiers, 9(6), 1777–1794.

[32]. Moraru, S.-S., Ene, A., & Badila, A. (2020). Physical and hydro-physical characteristics of soil in the context of climate change: A case study in Danube River Basin, SE Romania. Sustainability, 12(21), 9174.

[33]. Dewangan, S. K., Gupta, K., Kushwaha, A., & Chakraborty, P. (2024). Characterization of soil physical properties: Insights into texture, structure, and porosity. International Research Journal of Modernization in Engineering Technology and Science, 6, 2129–2135.

[34]. Thakur, P., Butail, N. P., Sankhyan, N. K., Kumar, N., Sharma, P., Thakur, P., & Kumar, P. (2024). Land use impacts hydro-physical attributes of soil. Himachal Journal of Agricultural Research, 50(2), 268–274.

[35]. Alkharabsheh, H. M., Seleiman, M. F., Battaglia, M. L., Shami, A., Jalal, R. S., Alhammad, B. A., Almutairi, K. F., & Al-Saif, A. M. (2021). Biochar and its broad impacts in soil quality and fertility, nutrient leaching and crop productivity: A review. Agronomy, 11(5), 993.

[36]. Dewangan, S. K., Jaiswal, P., & Kujur, A. (2025). Soil quality assessment based on physico-chemical parameters of white soil from Sonhat Block, District Koriya. International Journal of Research Publication and Reviews, 6(6), 7611–7616.

[37]. Veettil, A. V., Rahman, A., Awal, R., Fares, A., Melaku, N. D., Thapa, B., Elhassan, A., & Woldesenbet, S. (2024). Transforming soil: Climate-smart amendments boost soil physical and hydrological properties. Soil Systems, 8(4), 134.

[38]. Nazir, A., Hussain, S. M., Riyaz, M., Kere, Z., Zargar, M. A., & Dev, K. D. L. (2024). Environmental risk assessment, spatial distribution, and abundance of heavy metals in surface sediments of Dal Lake–Kashmir, India. Environmental Advances, 17, 100562.

[39]. Shi, Y., Xu, L., Ma, X., & Guo, J. (2025). Study on the organic geochemical characteristics of Jurassic source rocks from the Northern Tibetan Plateau Basin. Processes, 13(10), 3266.

[40]. de Groot, P. A. (2009). Stable isotope ratio analysis in geochemical processes. In Handbook of Stable Isotope Analytical Techniques, Elsevier, 881–928.

[41]. Balaram, V., & Subramanyam, K. S. V. (2022). Sample preparation for geochemical analysis: Strategies and significance. Advances in Sample Preparation, 1, 100010.

[42]. Chiozzi, V., Agriopoulou, S., & Varzakas, T. (2022). Advances, applications, and comparison of thermal (pasteurization, sterilization, and aseptic packaging) against non-thermal (ultrasounds, UV radiation, ozonation, high hydrostatic pressure) technologies in food processing. Applied Sciences, 12(4), 220.

[43]. Cheng, K. L., & Zhu, D.-M. (2005). On calibration of pH meters. Sensors, 5(4), 209–219.

[44]. Nowak, P. M., Biel, I., Kózka, G., Klag, M., & Woźniakiewicz, M. (2022). Influence of pH measurement inaccuracy on the values of acidity constant determined on the basis of electrophoretic and thermophoretic data. Microchemical Journal, 181, 107689.

[45]. Wu, Y. C., Koch, W. F., & Pratt, K. W. (1991). Proposed new electrolytic conductivity primary standards for KCl solutions. Journal of Research of the National Institute of Standards and Technology, 96(2), 191–205.

[46]. Liu, M., Wang, T., Yu, W., & Wang, J. (2007). An electrical conductivity probe method for measuring the local solid holdup in a slurry system. Chemical Engineering Journal, 132(1–3), 37–46.

[47]. Nedović, S., Alil, A., Martinović, S., Dikić, S., Glišić, D., & Volkov-Husović, T. (2025). Novel approach to the surface degradation assessment of 42CrMo4 steel in marine and cavitation erosion environments. Metals, 15(10), 1154.

[48]. Gibs, J., Wilde, F., & Heckathorn, H. (2007). Use of multiparameter instruments for routine field measurements (ver. 1.1). U.S. Geological Survey Techniques of Water-Resources Investigations, Book 9, Chapter A6, Section 6.8.

[49]. Mahato, N., Sinha, M., Sharma, K., Koteswararao, R., & Cho, M. H. (2019). Modern extraction and purification techniques for obtaining high purity food-grade bioactive compounds and value-added co-products from citrus wastes. Foods, 8(11), 523.

[50]. Kenig, E. Y. (1995). Mass transfer-reaction coupling in two-phase multicomponent fluid systems. The Chemical Engineering Journal and the Biochemical Engineering Journal, 57(2), 189–204.

[51]. Jin, H., Wang, E., Yuan, D., Zhang, W., & Li, H. (2025). Optimization of synchronous grout properties and construction parameters for shield tunnels in soft soil. Scientific Reports, 15, 26341.

[52]. Beaulieu, L. Y., Logan, E., Gering, K. L., & Dahn, J. R. (2017). An automated system for performing continuous viscosity versus temperature measurements of fluids using an Ostwald viscometer. Review of Scientific Instruments, 88(2), 025107.

[53]. Kumar, A., Bhawsar, N., Manekar, S., Pendram, B., Pal, P., Ali, D., Yadav, V. K. (2025). Extraction and optimization of lycopene from selected fruits and their assessment as an ultraviolet ray protectant for Escherichia coli. Food Science & Nutrition, 13(4), e70090.

[54]. Kumar, A., Singh, B., & Tyagi, K. (2014). Physicochemical analysis of PT.ET. extracted lycopene and viscosity, surface tension characterization by Mansingh Survismeter. World Journal of Pharmaceutical Research, 3(4), 778–784.

[55]. Shen, R., Liu, T., Liu, H., Zou, X., Gong, Y., & Guo, H. (2024). An enhanced vacuum-assisted resin transfer molding process and its pressure effect on resin infusion behavior and composite material performance. Polymers, 16(10), 1386.

[56]. Meshram, D., Thakkar, K., Dhara, P., & Patel, M. (2013). Evaluation of standards of some selected shampoo preparation. World Journal of Pharmacy and Pharmaceutical Sciences, 2(6), 3622–3630.

[57]. Godeto, Y. G., Bachheti, R. K., Bachheti, A., Saini, S., Wabaidur, S. M., Mohammed, A. A. A., Širić, I., Kumar, P., Abou Fayssal, S., & Rai, N. (2023). Sustainable Use of Extracts of Some Plants Growing in Ethiopia for the Formulation of Herbal Shampoo and Its Antimicrobial Evaluation. Sustainability, 15(4), 3189.